Electronic Supplementary Material (ESI) for Materials Horizons.

Mapping Mechanisms and Growth Regimes of Magnesium Electrodeposition at High Current Densities

Rachel Davidson,[a,b] Ankit Verma,[c] David Santos,[a,b] Feng Hao,[c] Cole Fincher,[d] Dexin Zhao,[b] Vahid Attari,[b,d] Parker Schofield, [a,b] Jonathan Van Buskirk,[a,b] Antonio Fraticelli-Cartagena,[a] Theodore E. G. Alivio,[a,b] Raymundo Arroyave,[b,d] Kelvin Xie,[b] Matt Pharr,[d] Partha P. Mukherjee,[c]* Sarbajit Banerjee [a,b] *

a) *Department of Chemistry, Texas A&M University, College Station, TX 77843, USA.*
b) *Department of Materials Science & Engineering, Texas A&M University, College Station, TX 77843, USA.*
c) *School of Mechanical Engineering, Purdue University, West Lafayette, IN 47907, USA.*
d) *Department of Mechanical Engineering, Texas A&M University, College Station, TX 77843, USA*

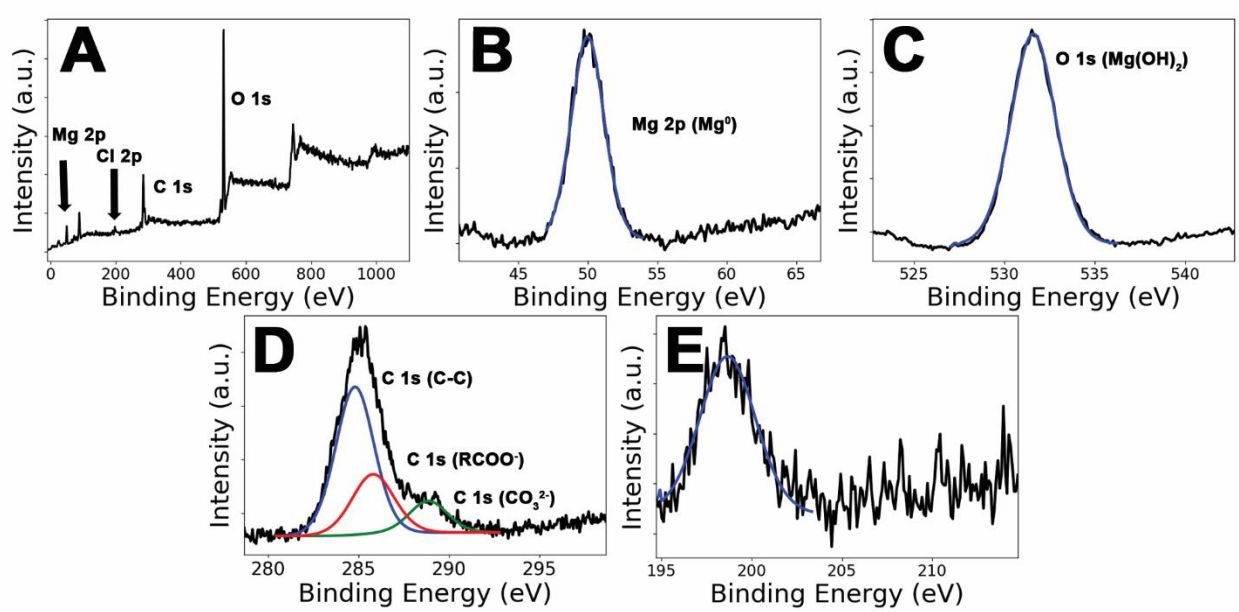

Figure S1. A) XPS survey scan measured for detached Mg fractal deposits formed at a current density of 0.921 mA/cm^2 from a 0.5M solution of MeMgCl in THF; High-resolution XPS spectra measured at B) Mg 2p; C) O 1s; D) C 1s regions; and E) high-resolution Cl 2p XPS spectrum. Spectral assignments are indicated for each of the deconvoluted lines.

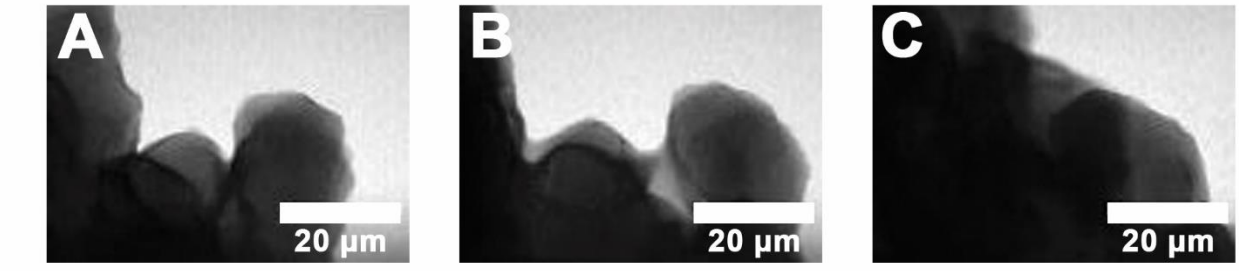

Figure S2. Projections of 3D tomographic maps from soft-X-ray microscopy at the Mg K-edge acquired at tilt angles of A) 40°, B) 80°, and C) 120°.

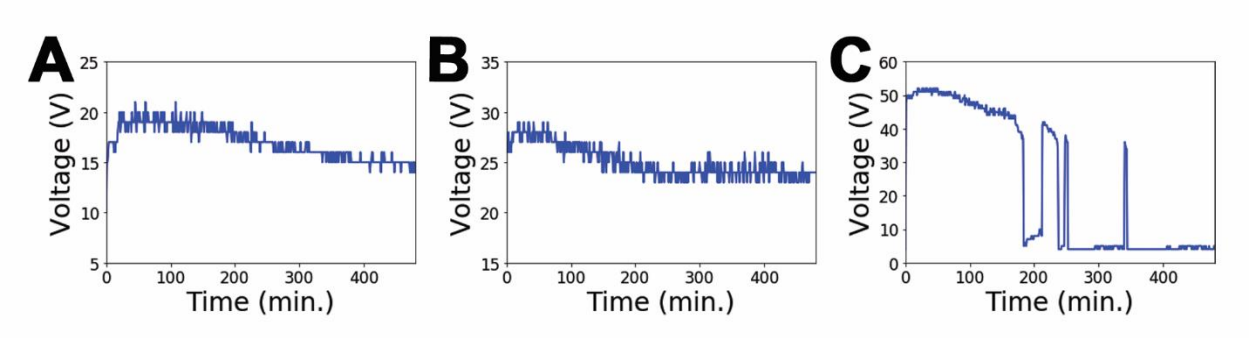

Figure S3. Plots of voltage *versus* time for the electrodeposition of Mg from MeMgCl as a function of applied current density for electrodeposition reactions at A) 0.307, B) 0.921, and C) 1.54 mA/cm^2 constant current applied for 8 h in 0.5 M MeMgCl solutions in THF.

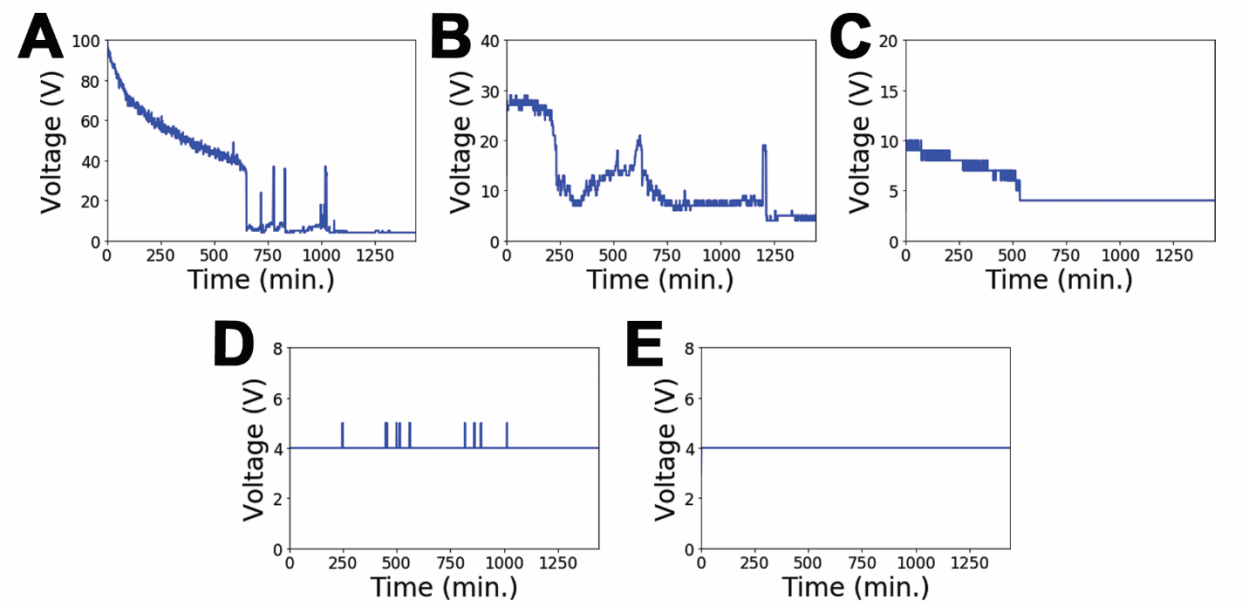

Figure S4. Plots of voltage *versus* time for the electrodeposition of Mg from MeMgCl as a function of concentration of electrolyte showing plots for reactions run with A) 0.25, B) 0.5, C) 1.0, D) 1.5, E) 2.0 M MeMgCl electrolyte solutions under a constant current of 0.921 mA/cm^2 applied for 24 h.

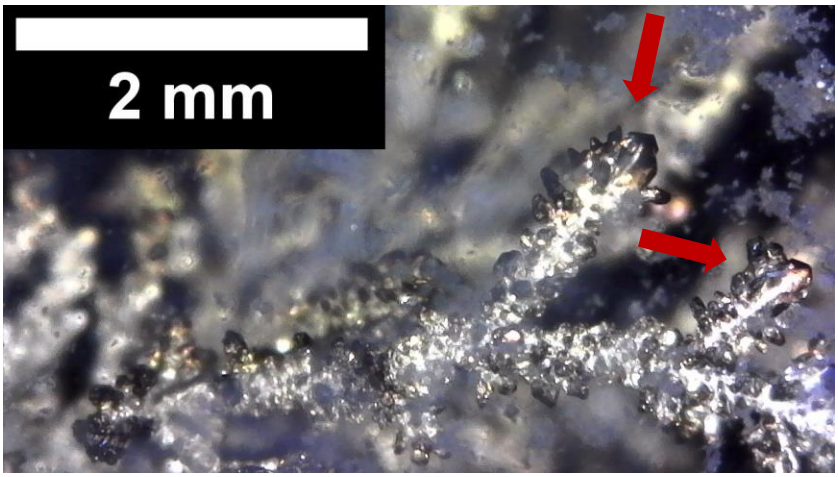

Figure S5. Digital image of a dendrite deposited under 0.921 mA/cm^2 applied current density in a 1.5 M MeMgCl solution for 24 h.

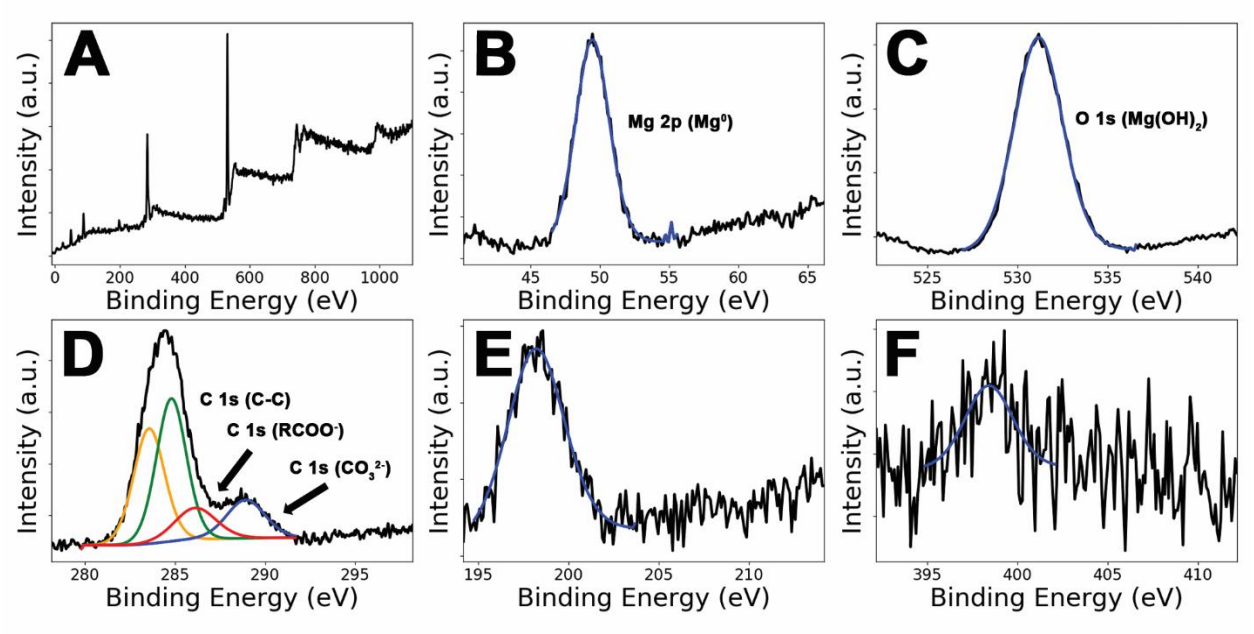

Figure S6. A) XPS survey scan measured for detached Mg fractal deposits formed at a current density of 0.921 mA/cm^2 from a 0.5M solution of MeMgCl in THF with the addition of oleylamine; High-resolution XPS spectra measured at B) Mg 2p; C) O 1s; D) C 1s regions; E) high-resolution Cl 2p XPS spectrum; and F) N 1s. Spectral assignments are indicated for each of the deconvoluted lines.

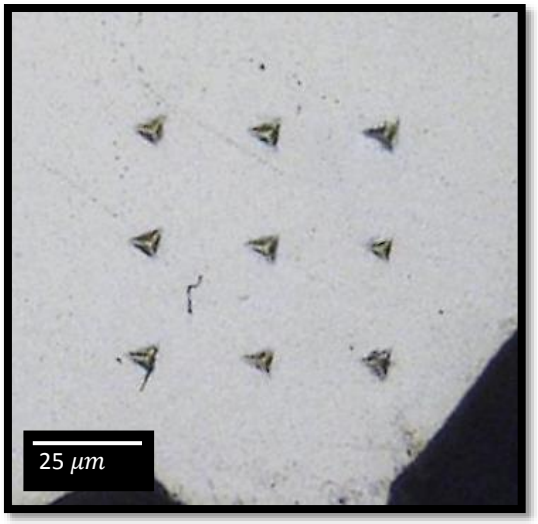

Figure S7. Optical image acquired for a set of indents in the cross-section of a polished Mg dendrite grown in 0.5 M MeMgCl solutions under 0.921 mA/cm^2 applied constant current for 24 h, displaying insignificant indentation pile-up.

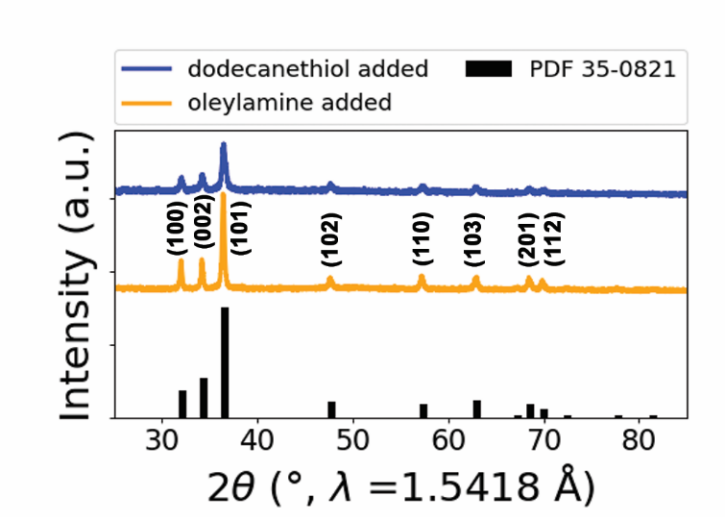

Figure S8. Powder XRD patterns for Mg deposits electrodeposited at a current density of 0.921 mA/cm^2 from 0.5M MeMgCl electrolyte solutions with the addition of dodecanethiol and oleylamine. The reflections can be indexed to metallic Mg with hexagonal close packing of atoms (PDF 35-0821).

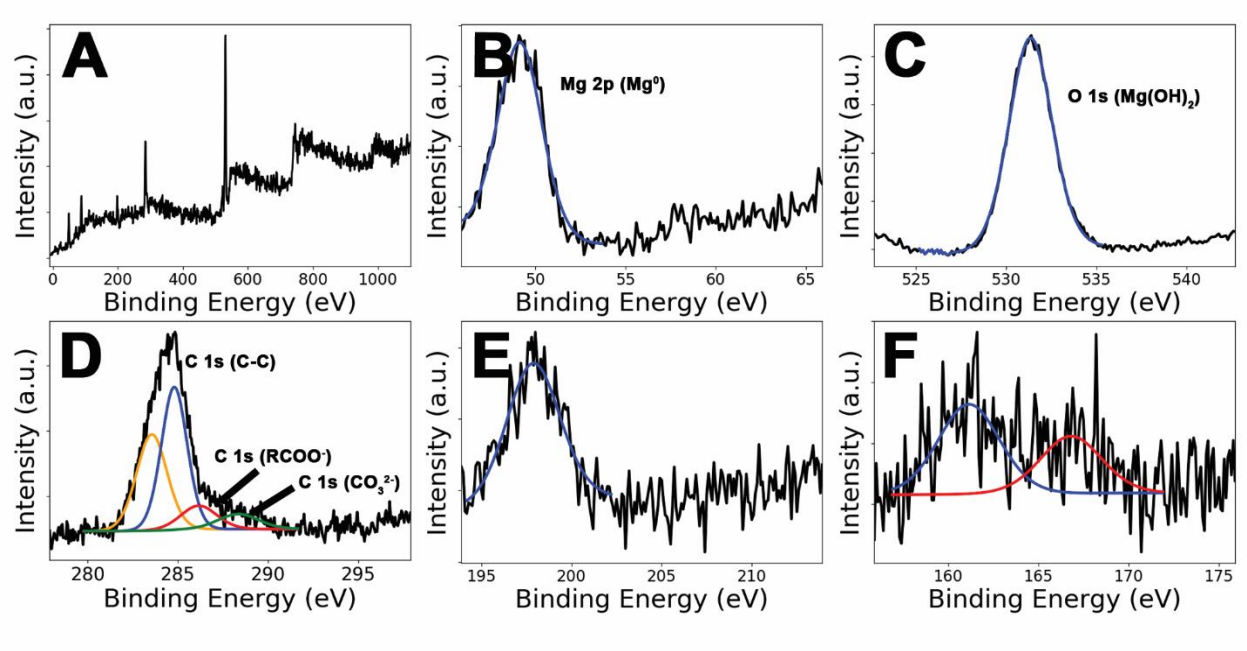

Figure S9. A) XPS survey scan measured for detached Mg fractal deposits formed at a current density of 0.921 mA/cm^2 from a 0.5M solution of MeMgCl in THF with the addition of dodecanethiol; High-resolution XPS spectra measured at B) Mg 2p; C) O 1s; D) C 1s regions; E) high-resolution Cl 2p XPS spectrum; and F) S 2p. Spectral assignments are indicated for each of the deconvoluted lines.

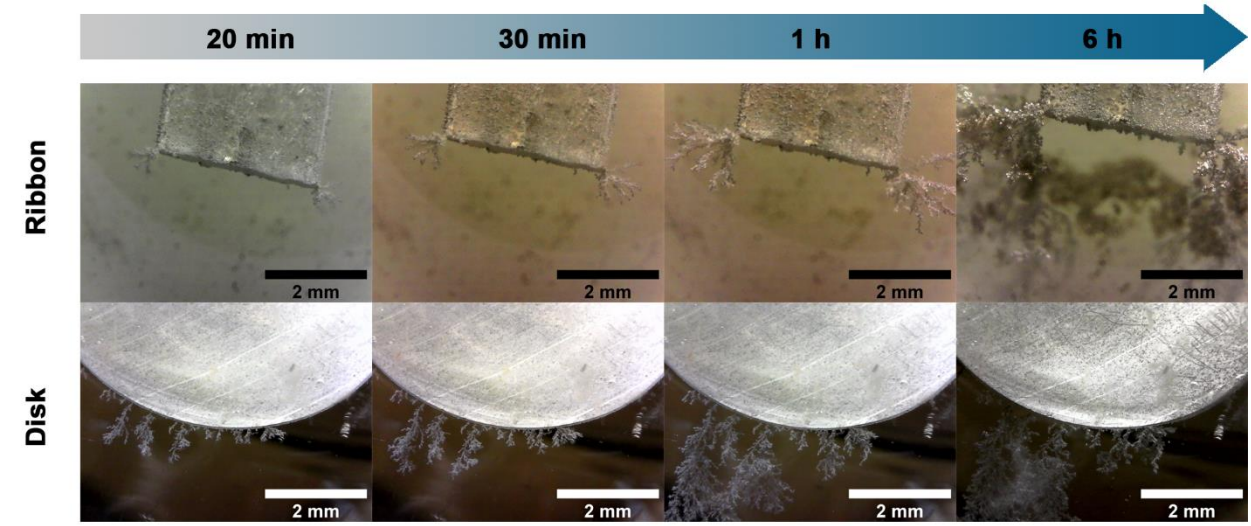

Figure S10. Digital images of an Mg ribbon and disk electrode as a function of time upon electrodeposition from a 0.5 M MeMgCl solution in THF under a 0.921 mA/cm^2 applied current density held constant for 24 h.

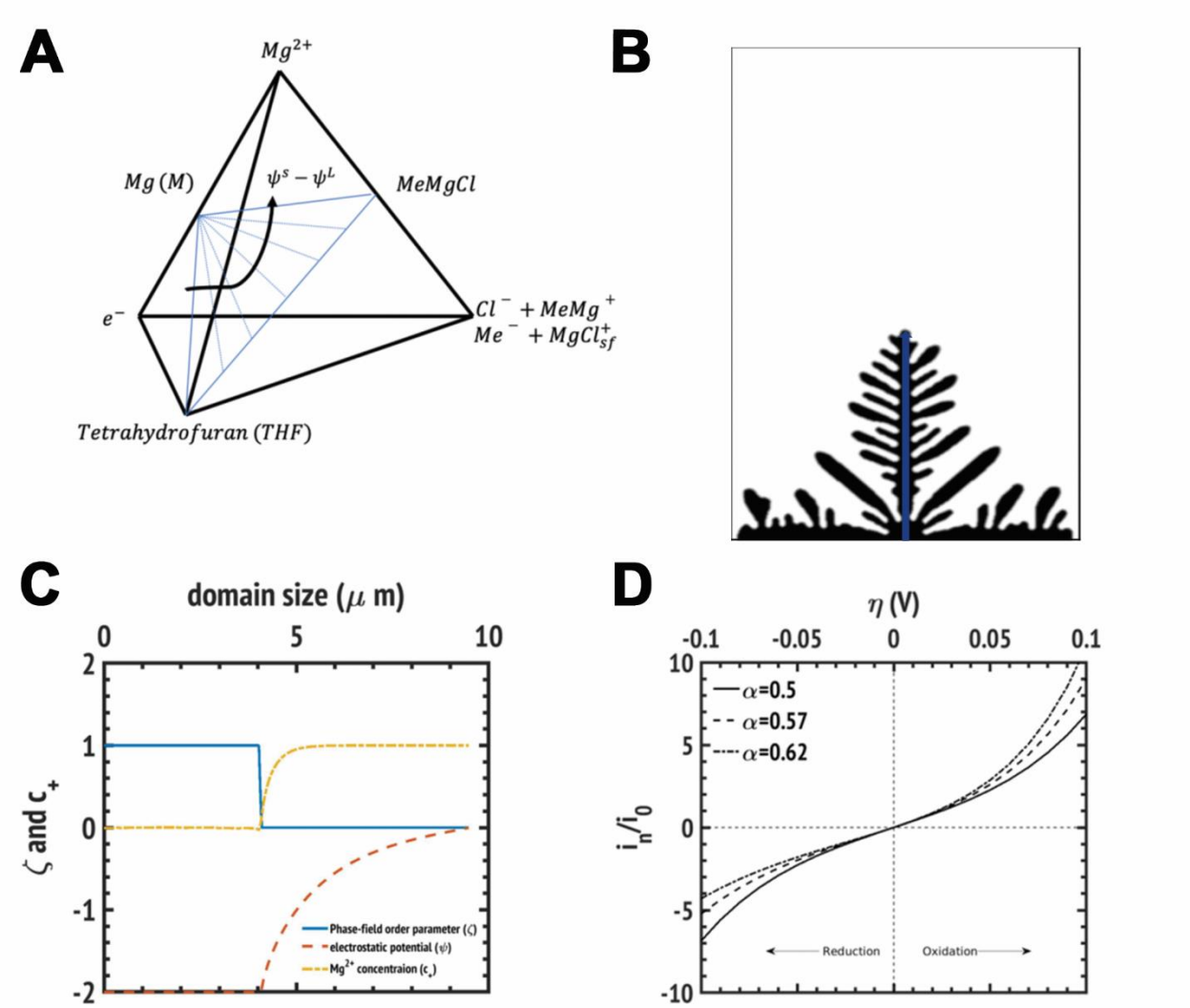

Figure S11. A) Hypothetical phase diagram and charge-neutral plane for Mg(M)-MeMgCl-THF. B) Dendrite formed following initial seeding at the bottom center of the domain. C) Phase-field order parameters extracted along the blue line in (B). D) Comparison of the nonlinear phase-field model with a Butler-Volmer symmetric coefficient of α=0.5 used in this study and Butler-Volmer coefficients reported by Viestfrid and co. workers[1] for (0.25 M complex in THF) and for (0.25 M complex in (0.25 M Bu_2Mg + THF) solutions.

Phase-field modeling of dendritic growth. The model described here was developed based on the earlier work of Guyer et. al[2], Bazant[3], Chen et al[4], and Yurkiv et al[5]. Primary deposition occurs through the reaction of M^{n+} cations in the electrolyte solution ($M^{n+}A^{n-}$) with electrons e^- at the surface of the electrode. In an isothermal and isobaric state, the total free energy of a heterogeneous system with constant volume V is given by:

$$F^{tot}(\zeta, c_i, \nabla c_i, \psi) = \int_V \left[f^{chem} + f^{int} + f^{elec} + f^{noise}\right] dV \qquad \text{(S1)}$$

where f^{chem}, f^{int}, f^{elec} and f^{noise} are the chemical, interfacial, electrical, and Langevin noise contributions respectively, given as:

$$f^{chem} = g(\bar{c}) + RT[\bar{c}_+ \ln(\bar{c}_+) + \bar{c}_- \ln(\bar{c}_-)] \quad \text{(S2)}$$

$$f^{int} = \frac{1}{2} \nabla c\kappa . \nabla c \quad \text{(S3)}$$

$$f^{elec} = \mathcal{F} \sum_i z_i c_i \psi \quad \text{(S4)}$$

$$f^{noise} = Ah'(\zeta)\chi \quad \text{(S5)}$$

where $g(\bar{c}) = W\bar{c}^2(1-\bar{c}^2) = W\zeta^2(1-\zeta^2)$ is a double well potential function with W being the barrier height of transformation in between the equilibrium states of the electrode and electrolyte. The second term in Eq. (S2) is the entropic contribution of mixing ions where R is the ideal gas constant, and T is the operating temperature. f^{int} describes the interfacial contributions due to heterogeneous nature of the electrode-electrolyte interface where the anisotropic characteristics of this interface was taken into account by:

$$\kappa(\theta) = \kappa_0(1 + \delta\cos[j\theta - \theta_0]) \quad \text{(S6)}$$

where δ and j are the strength and mode of anisotropy, respectively; κ_0 is the interface energy gradient, θ and θ_0 are related to the angle between the normal vector of the surface and the reference axis. f^{elec} is the electrostatic energy density, where $\mathcal{F}$ and z_i are the Faraday's constant and valence of species i, respectively. An additional phase-field variable was used to distinguish the states of the electrolyte ($\zeta = 0$) and electrode ($\zeta = 1$), which continuously changes in the interface region. f^{noise} denotes the Langevin noise, which was applied to the interface region by using χ, which is a quasi-random number between [-1,1], and A is the amplitude of the fluctuation. The evolution of the non-conserved, conserved, and electrostatic fields were prescribed by the following equations, respectively:

$$\frac{\partial \zeta}{\partial t} = -L_\sigma(g'(\zeta) - \kappa(\theta)\nabla^2\zeta) - \Gamma \quad \text{(S7)}$$

$$\frac{\partial c_+}{\partial t} = \nabla\left[D^{eff}\nabla c_+ + \frac{D^{eff}c_+}{RT} n\mathcal{F}\nabla\psi\right] - \frac{c_s}{c_0}\frac{\partial \zeta}{\partial t} \quad \text{(S8)}$$

$$\nabla[\sigma^{eff}\nabla\psi] = n\mathcal{F}c_s\frac{\partial \zeta}{\partial t} \quad \text{(S9)}$$

where L_σ is the interface mobility, and Γ is the electrodeposition rate defined by:

$$\Gamma = L_\eta i_0 h'(\zeta)\left\{e^{\frac{(1-\alpha)n\mathcal{F}\eta_a}{RT}} - c_+ e^{\frac{(\alpha)n\mathcal{F}\eta_a}{RT}}\right\} \quad \text{(S10)}$$

where L_η is the reaction related kinetic coefficient, i_0 is the exchange current density, h' is the derivative of the interpolation function $h(\zeta) = \zeta^3(10 - 15\zeta + 6\zeta^2)$, α is the anodic/cathodic symmetric charge-transfer coefficient (assumed to be 0.5 in this study ($0 < \alpha < 1$)), and η_a is the overpotential. D^{eff} and σ^{eff} are the interdiffusion and conductivity, respectively defined over the domain by means of the interpolation function $h(\zeta)$. The source term in Eq. (S9) is related to reaction rate.

Table S1. List of boundary conditions used for equations 7-9

	Eq. (7)	**Eq. (8)**	**Eq. (9)**
Top		$c = c^{electrolyte}$	$\boldsymbol{\nabla\psi = \Delta\psi_{half-cell}}$
Bottom	$\nabla\zeta = 0$	$c = c^{Mg^{2+}}$	$\boldsymbol{\nabla\psi = \Delta\psi_{anode}}$
Left/Right		$\nabla c = 0$	$\boldsymbol{\nabla\psi = 0}$

References:

(1) Viestfrid, Y.; Levi, M. D.; Gofer, Y.; Aurbach, D. Microelectrode Studies of Reversible Mg Deposition in THF Solutions Containing Complexes of Alkylaluminum Chlorides and Dialkylmagnesium. *J. Electroanal. Chem.* **2005**, *576* (2), 183–195.

(2) Guyer, J. E.; Boettinger, W. J.; Warren, J. A.; Mcfadden, G. B. *Phase Field Modeling of Electrochemistry II: Kinetics*; 2003.

(3) Bazant, M. Z. Theory of Chemical Kinetics and Charge Transfer Based on Nonequilibrium Thermodynamics. **2019**, *6*, 23.

(4) Chen, L.; Zhang, H. W.; Liang, L. Y.; Liu, Z.; Qi, Y.; Lu, P.; Chen, J.; Chen, L.-Q. Modulation of Dendritic Patterns during Electrodeposition: A Nonlinear Phase-Field Model. *J. Power Sources* **2015**, *300*, 376–385.

(5) Yurkiv, V.; Foroozan, T.; Ramasubramanian, A.; Shahbazian-Yassar, R.; Mashayek, F. Phase-Field Modeling of Solid Electrolyte Interface (SEI) Influence on Li Dendritic Behavior. *Electrochim. Acta* **2018**, *265*, 609–619.